Since January 2020 Elsevier has created a COVID-19 resource centre with free information in English and Mandarin on the novel coronavirus COVID-19. The COVID-19 resource centre is hosted on Elsevier Connect, the company's public news and information website.

Chemical Physics Letters 774 (2021) 138618

Contents lists available at ScienceDirect

Chemical Physics Letters

journal homepage: www.elsevier.com/locate/cplett

Research paper

In silico investigation of potential small molecule inhibitors of the SARS-CoV-2 nsp10-nsp16 methyltransferase complex

Julia Liang [a,b], Eleni Pitsillou [a,b], Lucy Burbury [a,c], Andrew Hung [b], Tom C. Karagiannis [a,d,*]

[a] Epigenomic Medicine, Department of Diabetes, Central Clinical School, Monash University, Melbourne, VIC 3004, Australia
[b] School of Science, College of Science, Engineering & Health, RMIT University, VIC 3001, Australia
[c] Department of Microbiology and Immunology, The University of Melbourne, Parkville, VIC 3052, Australia
[d] Department of Clinical Pathology, The University of Melbourne, Parkville, VIC 3052, Australia

ARTICLE INFO

Keywords:
Coronavirus
COVID-19
SARS-CoV-2
Molecular docking
Nsp10
Nsp16
Methyltransferase

ABSTRACT

The COVID-19 pandemic caused by SARS-CoV-2 has resulted in an international health emergency. The SARS-CoV-2 nsp16 is an S-adenosyl-L-methionine (SAM)-dependent methyltransferase, and with its cofactor nsp10, is responsible for RNA cap formation. This study aimed to identify small molecules binding to the SAM-binding site of the nsp10-nsp16 heterodimer for potential inhibition of methyltransferase activity. By screening a library of 300 compounds, 30 compounds were selected based on binding scores, side-effects, and availability. Following more advanced docking, six potential lead compounds were further investigated using molecular dynamics simulations. This revealed the dietary compound oleuropein as a potential methyltransferase inhibitor.

1. Introduction

The ongoing coronavirus disease 2019 (COVID-19) pandemic caused by severe acute respiratory syndrome coronavirus 2 (SARS-CoV-2) continues to pose significant public health concerns, having caused millions of infections worldwide and devastating global economies [1]. The development of a safe and effective vaccine against COVID-19 remains a priority, with a global effort culminating in numerous clinical trials underway [2]. There has also been interest in the investigation of potential prophylactic and therapeutic compounds, with drug repurposing presenting an expedited avenue of COVID-19 suppression through utilising existing medications for which dosages and side effects are known. Remdesivir, an inhibitor of the viral RNA-dependent RNA polymerase, was approved by the Food and Drug Administration (FDA) for emergency use authorisation of hospitalised COVID-19 patients with severe disease [3]. However, clinical trial data has shown that benefits of remdesivir were modest to none on survival, particularly for moderately ill patients [4,5]. More controversially, the emergency use authorisation of the antimalarial drug hydroxychloroquine for treating patients with COVID-19 was initially provided, and then revoked following findings it was ineffective in reducing mortality [6]. In the absence of an efficacious treatment for COVID-19, a greater understanding of the pathogenesis and potential interventions is required.

Coronaviruses are a family of enveloped positive-sense single-stranded RNA viruses belonging to the family *Coronaviridae* [7]. Human coronaviruses, such as HCoV-229E, HCoV-OC43, HCoV-NL63, and HCoV-HKU1, are known to circulate in the population and are mildly pathogenic, causing seasonal common cold-like symptoms [7]. Conversely, the highly pathogenic severe acute respiratory syndrome coronavirus (SARS-CoV) and Middle East respiratory virus syndrome coronavirus (MERS-CoV) epidemics emerged in 2003 and 2012 respectively, with infections that can develop into life-threatening pathologies [7,8]. While the closely related SARS-CoV-2 has a lower mortality rate, it has a far higher transmissibility leading to difficulties in containment [8].

The genome of SARS-CoV-2 has ~29,800 bases, with 14 open reading frames (ORFs) encoding four structural and 16 non-structural proteins (nsp1 to nsp16) [9]. At the 5′ terminus of the genome, the ORF1ab and ORF1a genes encode polyproteins pp1ab and pp1a, while the 3′-terminus encodes four major structural proteins, including the spike surface glycoprotein [9]. Following entry of SARS-CoV-2 into the host cell, the polyproteins are translated and processed into the 16 nsps, 15 of which are assembled into the replication transcription complex (RTC) [7]. The RTC assembly is comprised of enzymes that maintain the

* Corresponding author at: Head Epigenomic Medicine Program, Department of Diabetes, Central Clinical School, Monash University, Melbourne, VIC 3004, Australia.
E-mail address: tom.karagiannis@monash.edu (T.C. Karagiannis).

https://doi.org/10.1016/j.cplett.2021.138618
Received 25 November 2020; Received in revised form 1 April 2021; Accepted 5 April 2021
Available online 9 April 2021

integrity of the coronavirus genome through regulating RNA proofreading, as well as RNA-processing and RNA-modification [7]. Within this complex, nsp14 and nsp16 are responsible for capping viral mRNA, which serves the critical function of avoiding innate immune recognition by the host [10]. In concert with nsp10, nsp16 converts mRNA species from a Cap-0 to Cap-1 structure through 2′-O methylation of the first transcribed nucleotide [11]. This process is dependent on the use of S-adenosyl-L-methionine (SAM) as the methyl donor [12]. Nsp10 is a necessary cofactor for nsp16 function, inducing a conformational change to stabilise the SAM-binding pocket [13].

In addition to synthesised drugs, there has been interest in the investigation of antiviral activity of naturally-occurring compounds derived from dietary sources [14]. Extra-virgin olive oil is the principal source of dietary fat in the Mediterranean diet, with bioactive properties attributable to its phenolic compound content [15]. It is hypothesised that small molecules may potentially inhibit methyltransferase activity of the SARS-CoV-2 nsp10-nsp16 complex by binding to the SAM-binding site. The SARS-CoV-2 nsp16 has been an attractive target for small molecule inhibition [16]. In the present study, we screened a library of 300 ligands for potential inhibitors of the SARS-CoV-2 nsp10-nsp16 methyltransferase complex using molecular docking. A majority of these compounds were derived from the olive, consisting of 220 phenolic compounds and 13 fatty acids obtained from the OliveNet^{TM} Library, as well as a selection of additional small molecules with known antiviral, antioxidant, and anti-inflammatory activities [17]. Via molecular docking studies, we identified several lead compounds that may be suitable for further analysis as potential inhibitors of SARS-CoV-2 methyltransferase activity.

2. Materials and methods

2.1. Protein structures and ligands

The crystal structure of the SARS-CoV-2 nsp10-16 methyltransferase complex was obtained from the RCSB Protein Data Bank (PDB ID: 6YZ1) [13]. Crystallographic waters and ligands were removed, and the native zinc ions were retained. 300 small molecules were chosen for investigation against the nsp10-nsp16 methyltransferase complex. 233 of these were obtained from the OliveNet^{TM} Library [17], including 220 phenolic compounds and 13 fatty acids. Additional ligands included known protease inhibitors and antibiotics, and compounds with proven antiviral, antioxidant and anti-inflammatory properties [18–25]. Compounds that were screened against the nsp10-nsp16 methyltransferase complex are listed in Table S1. Ligand structures were obtained from the National Centre for Biotechnology Information PubChem database [26]. Chem3D 19.0 (Perkin Elmer, Massachusetts, USA) was used to draw unavailable ligand structures.

2.2. Molecular docking using the Schrödinger Suite

Structure preparation and molecular docking was performed using the Schrödinger Suite (version 2020-2) molecular modelling package. The nsp10-nsp16 methyltransferase complex was prepared using the Protein Preparation Wizard, and ligands were processed using LigPrep. Initial screening of all 300 compounds utilised Glide for molecular docking with the standard precision mode (SP) selected. Docking was performed using default settings, utilising the OPLS3e force field. The receptor grid was centred around the co-crystallised sinefungin and was 20 × 20 × 20 Å in size. 30 compounds were selected for further analysis based on binding affinity, known side effects, and availability.

For the top 30 compounds, molecular docking was subsequently performed using the quantum-mechanics-polarised ligand docking (QPLD) protocol of the Schrödinger Suite as previously described [27,28]. The receptor grid was centred around the co-crystallised sinefungin and was 20 × 20 × 20 Å in size.

2.3. Ligand binding site identification and blind docking of top compound

The PrankWeb server was used to identify potential ligand binding sites in the nsp10-nsp16 protein complex [29]. Blind docking of 30 compounds selected based on initial screening was performed using AutoDock Vina [30]. The receptor grid encompassed the entire surface of the heterodimer, and docking was performed at an exhaustiveness of 2048. Blind docking calculations were performed using cloud computing services provided by Galileo (Hypernet Labs) [31].

2.4. Molecular dynamics simulations

Classical MD simulations with SARS-CoV-2 nsp10-nsp16 methyltransferase complex bound with small molecules were performed as previously described [27] using GROMACS 2018.2 software [32,33] and the CHARMM36 force field [34]. The starting structure of the SARS-CoV-2 nsp10-nsp16 protein complex was obtained from RCSB Protein Data Bank (PDB ID: 6YZ1) [13]. The native crystallised sinefungin, and docked dietary compounds oleuropein, oleacein, cyanidin-3-O-glucoside, and epigallocatechin gallate bound to the SAM-binding site was used as starting structures. Ligand topologies were generated with SwissParam [35]. Systems were fully solvated with TIP3P water in a dodecahedral box, with a minimum distance of 2.0 nm between protein atoms and the closest box edge. Simulations were performed with a time-step of 2 fs in triplicate for 200 ns, with trajectories totalling 3.6 μs across six separate systems. Root mean square fluctuation (RMSF) and contacts analysis was calculated for each complex between 50 and 100 ns of the stabilised trajectories. The number of contacts between the ligand and protein complex was calculated using gmx mindist, with a threshold of 0.45 nm used to define a contact between the ligand and protein residue [32,33].

3. Results and discussion

Mediated by the nsp10-nsp16 heterodimer, 2′-O-methylation is essential for RNA cap formation in SARS-CoV-2, which is critical for evading immune response in the host [36]. Thus, the nsp10-nsp16 methyltransferase complex is an attractive target for small molecule inhibition. The crystal structure of SARS-CoV-2 nsp10-nsp16 in complex with sinefungin, a pan-methyltransferase inhibitor, has been reported by Krafcikova et al., and was utilised in this study [13]. The co-crystallised sinefungin and the methyl donor SAM were used as controls.

3.1. Overall structure and predicted ligand binding site

The structure of the nsp10-nsp16 heterodimer is shown in Fig. 1A. Nsp10 is a necessary cofactor for the proper function of the

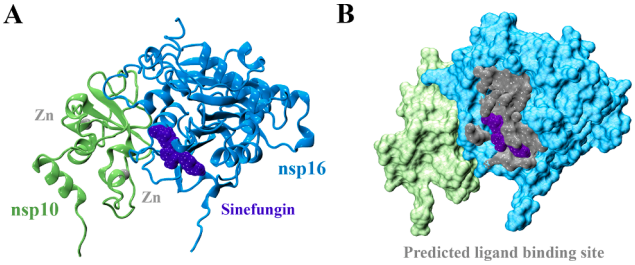

Fig. 1. Structure of SARS-CoV-2 nsp10-nsp16 methyltransferase complex. A) The nsp16 protein (blue) is bound to its cofactor nsp10 (green) to form a heterodimer (PDB ID: 6YZ1). Nsp10 contains two zinc (silver) binding sites. Crystallographic sinefungin (purple) illustrates the location of the active SAM-binding pocket. B) The top ranked predicted ligand binding site is highlighted in surface representation (silver), and is shown to encompass the active pocket surrounding sinefungin (purple). (For interpretation of the references to color in this figure legend, the reader is referred to the web version of this article.)

methyltransferases nsp14 and nsp16 [11]. Nsp10 contains two zinc binding sites, which stabilises helices α2 and α3, and the C-terminus of nsp10 [13]. Upon binding to nsp10, nsp16 promotes binding to the methyl donor SAM and capped RNA substrate [12]. The transfer of the methyl group from SAM to Cap-0 is catalysed by nsp16, to generate the reaction products S-adenosylhomocysteine (SAH) and Cap-1. Sinefungin binds within the SAM-binding pocket to inhibit this reaction, and is used as a pan-inhibitor of methyltransferases [37]. Fig. 1B depicts the top ranked potential ligand binding sites on the surface of the nsp10-nsp16 heterodimer using the PrankWeb server [29]. The top ranking pocket depicted yielded a binding site score of 20.7, compared to pockets ranked 2 to 9 having Site scores of less than 5. It is noted that the top ranked predicted ligand binding site encompasses the SAM-binding site, as well as extending into a groove that encroaches into the RNA binding groove. The predicted ligand binding site encompasses several residues involved in the stabilisation of RNA cap binding, such as Cys25, Tyr30, Lys137, and Ser202 [38].

3.2. Identification of lead compounds

In order to identify potential inhibitors, a library of 300 compounds were screened in this study using molecular docking. This library consisted of a combination of dietary compounds and known antivirals. An emphasis was placed on dietary compounds, particularly on phenolics from the OliveNet™ Library, a database of compounds derived from *olea europaea* we previously curated [17]. The 300 compounds were docked to the SAM-binding site of nsp16 in the heterodimer using Glide, with binding affinities shown in Table S1.

Based on binding affinities, known side effects, and availability, 30 compounds were selected for further investigation. The structures of these compounds are shown in Table S2. A more in-depth molecular docking study was performed with the top 30 compounds using the QPLD protocol of Schrodinger. QPLD incorporates Glide with mixed quantum mechanical/molecular mechanics (QM/MM) methods to determine ligand charges, yielding a more accurate docking method [39]. The top 30 compounds were also docked using blind docking, where the receptor grid encompassed the entire surface of the protein. This was performed in order to identify potential sites where the ligands would bind, with preferential binding of lead compound the active SAM-binding pocket. QPLD and blind docking results for the top 30 compounds are shown in Table 1.

Taking together the docking and blind docking results, 6 lead compounds were identified that may serve as the basis for further investigation as potential methyltransferase inhibitors. These were the antivirals lopinavir and ritonavir, and the dietary compounds oleuropein, oleacein, cyanidin-3-O-glucoside, and epigallocatechin gallate (EGCG). QPLD docking results are shown in Fig. 2 for the controls and antivirals, and Fig. 3 for the lead dietary compounds. The blind docking results for controls and antiviral compounds can be seen in Fig. 4, and blind docking results for dietary compounds in Fig. 5.

3.3. Sinefungin and SAM

SAM is the methyl donor substrate necessary for 2′-O methylation activity in nsp16, while sinefungin is a pan-methyltransferase inhibitor initially isolated from *Streptomyces griseoleus* [13,40]. Both these compounds were utilised as controls in the present study. In principal, small molecules binding with a greater affinity compared to SAM may be potential methyltransferase inhibitors.

From the QPLD docking results, SAM binds with a GlideScore of −9.6 kcal/mol, while sinefungin produced a slightly stronger score of −10.2 kcal/mol, in line with its known activity as a methyltransferase inhibitor (Fig. 2). Following docking to the SAM-binding site, sinefungin and SAM were observed to form hydrogen bonds with several highly conserved residues among SARS-CoV-2, SARS-CoV, and MERS, namely Asn43, Asp99, Asp114, Asp130, and Lys170 (Fig. 2) (13). Further, salt bridge formation was observed in the docked poses with Asp130 for both SAM and sinefungin, and Asp114 for sinefungin. The binding of these ligands with these key residues are in line with those reported by Krafcikova et al., who postulate that the proximity of the SAM-binding pocket to a putative RNA binding site may explain how nsp16 performs 2′-O methylation [13]. Nsp16 contains the highly conserved canonical catalytic K-D-K-E motif comprising of residues Lys46, Asp130, Lys170, and Glu203 [11,37,41]. This catalytic tetrad is in proximity to the SAM methyl group that is transferred to the 2′-OH on the methylated Cap-0 [37]. It is noted that as well at both SAM and sinefungin forming interactions with Asp130, sinefungin also formed a hydrogen bond with the catalytic Lys170.

When blind docking was performed, sinefungin and SAM produced 17 and 18 poses out of 20 in the SAM-binding pocket, respectively (Fig. 4). The top ranked pose for sinefungin produced a binding affinity of −7.7 kcal/mol, and a similar affinity was observed for SAM at −7.5

Table 1
The 30 compounds selected for further analysis based on initial screening. Compounds were docked to the SAM-binding site using the QPLD protocol, with GlideScores shown. Blind docking was performed to generate a maximum of 20 poses. The number of generated poses located in the SAM-binding site are listed, as well as its strongest ranked binding affinity. SAM and sinefungin were used as controls.

Compound	Classification	QPLD GlideScore (kcal/mol)	Number of poses in SAM-binding site	Top pose binding affinity (kcal/mol)
(-)Epicatechin gallate	Dietary	−10.3	10	−7.5
Amikacin	Antibiotic	−9.5	15	−7.2
Baricitinib	Janus kinase inhibitor	−7.8	17	−8.2
Cefotaxime	Antibiotic	−6.5	15	−7.2
Ceftazidime	Antibiotic	−5.6	14	−8.5
Ceftriaxone	Antibiotic	−7.4	20	−8.7
Cefuroxime	Antibiotic	−4.8	16	−7.0
Comselogoside	OliveNet™	−10.7	12	−8.4
Curcumin	Dietary	−7.2	13	−7.2
Cyanidin-3-O-glucoside	OliveNet™	−10.2	13	−8.4
Doripenem	Antibiotic	−4.8	18	−7.1
Epigallocatechin gallate	Dietary	−10.1	15	−7.6
Ertapenem	Antibiotic	−7.5	18	−9.2
GSK126	MTase inhibitor	−5.9	14	−9.5
GSK343	MTase inhibitor	−6.3	19	−9.0
Hellicoside	OliveNet™	−13.8	19	−9.1
Hesperidin	OliveNet™	−11.4	18	−9.1
Indinavir	Protease inhibitor	−6.6	18	−8.4
Lopinavir	Protease inhibitor	−8.0	19	−7.8
Nelfinavir	Protease inhibitor	−7.4	17	−8.0
Oleacein	OliveNet™	−7.9	9	−6.9
Oleohydroxypyretol	OliveNet™	−6.7	10	−6.5
Oleuropein	OliveNet™	−11.1	18	−6.8
Ritonavir	Protease inhibitor	−6.1	17	−8.3
Rutin	OliveNet™	−9.6	18	−8.1
SAM	Control	−9.6	18	−7.5
Sinefungin	Control	−10.2	17	−7.7
SRT1720	Sirtuin activator	−6.2	8	−8.8
SRT2104	Sirtuin activator	−5.2	11	−8.2
Suspensaside	OliveNet™	−14.2	19	−9.1
Tobramycin	Antibiotic	−8.0	10	−6.5
Verbascoside	OliveNet™	−9.8	20	−8.4

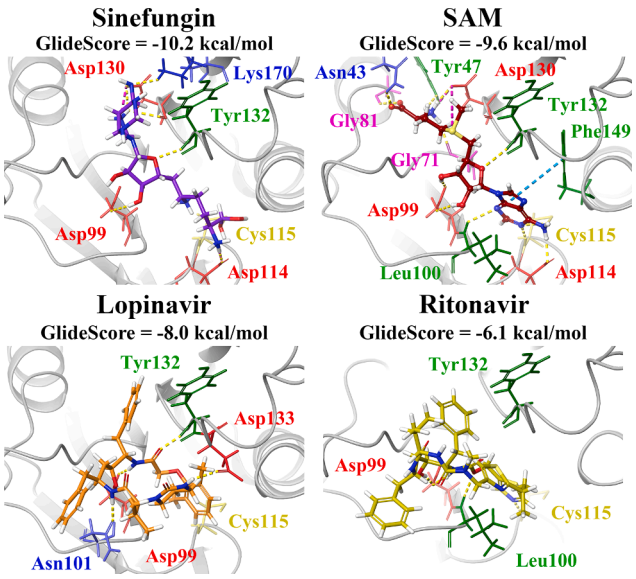

Fig. 2. Docking of controls and lead antiviral compounds to the SAM-binding pocket of SARS-CoV-2 nsp10-nsp16 methyltransferase complex. Control and lead antiviral compounds were docked to the active site of nsp10-nsp16 using the QPLD protocol of Glide. Residue interactions are shown as dashed lines, including hydrogen bonds (yellow), salt bridges (magenta), and π-π πinteractions (cyan). Amino acid residues are coloured according to their properties, namely hydrophobic residues (green), negatively charged residues (red), positively charged residues (blue), and glycine residues (pink). (For interpretation of the references to color in this figure legend, the reader is referred to the web version of this article.)

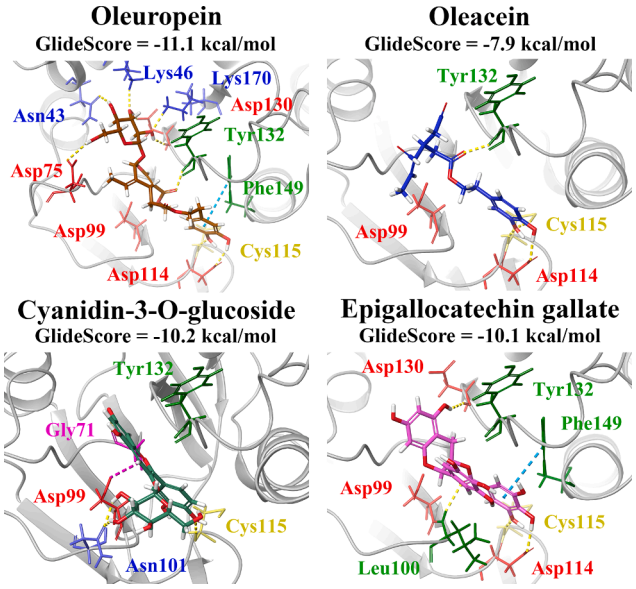

Fig. 3. Docking of lead dietary compounds to the SAM-binding pocket of SARS-CoV-2 nsp10-nsp16 methyltransferase complex. Lead dietary compounds were docked to the active site of nsp10-nsp16 using the QPLD protocol of Glide. Residue interactions are shown as dashed lines, including hydrogen bonds (yellow), salt bridges (magenta), and π-π interactions (cyan). Amino acid residues are coloured according to their properties, namely hydrophobic residues (green), negatively charged residues (red), positively charged residues (blue), and glycine residues (pink). (For interpretation of the references to color in this figure legend, the reader is referred to the web version of this article.)

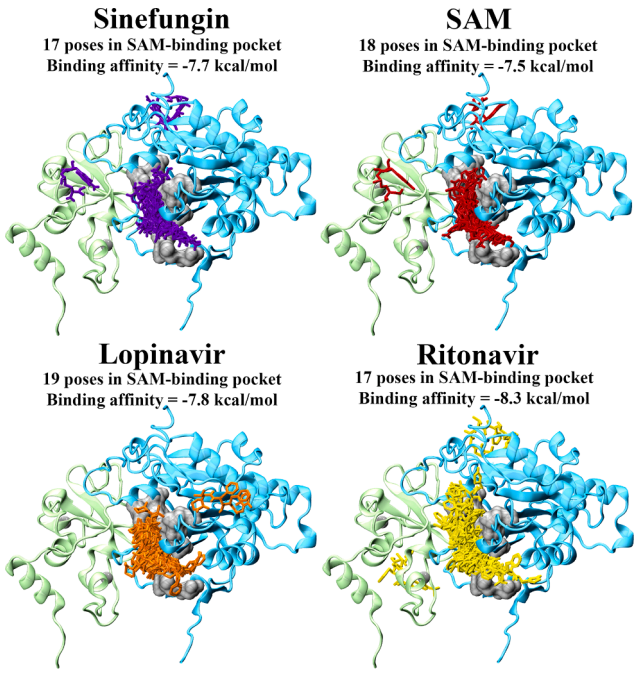

Fig. 4. Blind docking of control and lead antiviral compounds to SARS-CoV-2 nsp10-nsp16 methyltransferase complex. Blind docking was performed using AutoDock Vina to produce a maximum of 20 poses. The number of poses in the active SAM-binding pocket are listed for each compound, along with the binding affinity of the top ranked pose in the active site. Key residues of the SAM-binding pocket are shown in surface representation (silver).

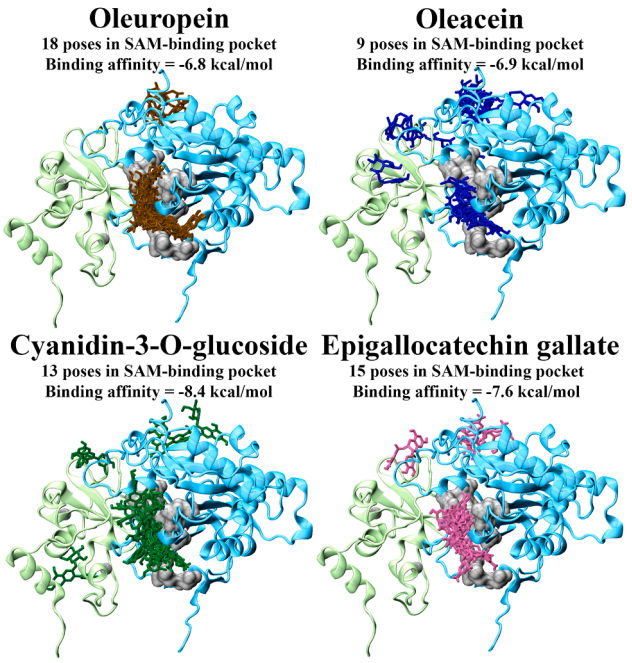

Fig. 5. Blind docking of lead dietary compounds to SARS-CoV-2 nsp10-nsp16 methyltransferase complex. Blind docking was performed using AutoDock Vina to produce a maximum of 20 poses. The number of poses in the active SAM-binding pocket are listed for each compound, along with the binding affinity of the top ranked pose in the active site. Key residues of the SAM-binding pocket are shown in surface representation (silver).

kcal/mol. These results reinforce the strong affinity of sinefungin and SAM to the active pocket of nsp16.

3.4. Lopinavir and ritonavir

Lopinavir-ritonavir has been studied as an antiviral treatment for patients with COVID-19 in clinical trials [42,43]. Lopinavir is a HIV-1 protease inhibitor, usually combined with ritonavir to increase plasma concentration and efficacy [42,43]. Lopinavir is an inhibitor of the SARS-CoV main protease, an enzyme necessary for viral replication and is highly conserved in SARS-CoV-2 [42,43]. Ritonavir is another protease inhibitor, inhibiting hepatic cytochrome P450 activity to increase plasma half-life [42]. While lopinavir/ritonavir has not been recommended as a treatment for COVID-19 beyond the context of clinical trials, the identification of these compounds as strong binders suggest that they may potentially have methyltransferase inhibition activity in addition to their known protease inhibitory properties.

Lopinavir and ritonavir bound to the SAM-binding site with GlideScores of −8.0 and −6.1 kcal/mol respectively (Fig. 2). Both compounds were observed to form hydrogen bonds with the conserved Asp99, lopinavir forming a hydrogen bond with the conserved Asn101 [13]. From blind docking, almost all produced poses were in the SAM-binding site for both lopinavir and ritonavir (Fig. 4). Lopinavir produced 19 out of 20 poses in the active pocket, while ritonavir had 17 active poses. In contrast to the QPLD results, ritonavir bound with a stronger affinity than lopinavir in blind docking with AutoDock Vina (-8.3 and −7.8 kcal/mol for ritonavir and lopinavir, respectively).

3.5. Oleuropein and oleacein

Oleuropein and oleacein are dietary compounds derived from the olive, classified as secoiridoids [17]. Oleuropein is one of the main polyphenolic constituents of olive oil and is widely recognised in the literature for its potent antioxidant activity and anti-inflammatory activity, with pharmacological activity in a wide range of diseases [44]. Oleacein has been suggested to possess methyltransferase inhibitory activity, functioning as a dual substrate-inhibitor of catechol-O-methyltransferase for potential anticancer activity [45]. It has also been hypothesised that oleacein may act as an inhibitor of lysine-specific histone demethylase 1A (LSD1), an epigenetic regulator of metabolic disorders and cancer [46].

QPLD docking revealed that oleuropein was among the strongest binding compounds to the SAM-binding site, with a GlideScore of −11.1 kcal/mol; stronger than the positive controls (Figs. 2 and 3). Hydrogen bonds were observed to form with the conserved Asn43 and Asn101, as well as with three of the four catalytic dyad residues: Lys46, Asp130, and Lys170 [13,38]. Additionally, 18 out of 20 poses were shown to bind to the SAM-binding pocket (Fig. 5). These results suggest that oleuropein may be a strong lead warranting further investigation. Oleacein bound to the active site with a GlideScore of −7.9 kcal/mol, forming hydrogen bonds with Cys115, Tyr132, and the conserved Asp114 [13]. From blind docking, 9 out of 20 poses for oleacein were binding to the SAM-binding pocket, with the top ranked pose binding with a similar affinity to that of oleuropein (−6.9 and −6.8 kcal/mol for oleacein and oleuropein, respectively) (Fig. 5).

3.6. Cyanidin-3-O-glucoside and EGCG

Cyanidin-3-O-glucoside and EGCG are also dietary derived compounds that were identified as leads with potential inhibition of methyltransferase activity. Cyanidin-3-O-glucoside is found in a variety of fruits and legumes, and is the main active anthocyanin in blueberry extracts [17,47]. Cyanidin-3-O-glucoside has been reported to have potential benefits in a variety of inflammatory diseases and cancer, including the attenuation of acute lung injury in rats with sepsis [47]. EGCG is an abundant catechin found in green tea, and has been heavily studied as for its antioxidant and chemopreventative properties [48].

Both cyanidin-3-O-glucoside EGCG bind strongly to the SAM-binding site of nsp16 with an affinity similar that of the controls, with GlideScores of −10.2 and −10.2 kcal/mol for cyanidin-3-O-glucoside and EGCG, respectively (Fig. 3). Cyanidin-3-O-glucoside forms a salt bridge to the conserved Asp99, and forms two hydrogen bonds with the conserved Asn101. EGCG forms a hydrogen bond with the conserved Asp114 and the catalytic Asp130. Pi-pi stacking is also observed with Phe149, which has been implicated in binding of SAM [12]. From blind docking, it was determined that the majority of poses produced were located in the SAM-binding site for both compounds, with 13 poses for cyanidin-3-O-glucoside and 15 poses for EGCG with stronger affinities than SAM (−8.4 and −7.6 kcal/mol for cyanidin-3-O-glucoside and EGCG, respectively (Fig. 5).

3.7. Stability of lead compounds bound to the active site of SARS-CoV-2 nsp10-nsp16 methyltransferase complex

To assess the stability of lead compounds bound to the SAM-binding pocket of SARS-CoV-2 nsp10-nsp16 methyltransferase complex, MD simulations were performed in triplicate for 200 ns (Figs. 6 and 7). A total of six different systems were studied: the apo protein complex, and the protein complex bound with the control compound sinefungin, and dietary compounds oleuropein, oleacein, cyanidin-3-O-glucoside, and epigallocatechin gallate (Movies S1 – S7). While molecular docking data suggested that all studied compounds were potential leads, visual analysis of MD trajectories show that sinefungin and oleuropein are the strongest binding compounds, remaining bound to the SAM-binding site of the nsp10-nsp16 methyltransferase complex (Movies S2 and S3). While epigallocatechin gallate remains bound to the active site for two of the repeat simulations, ligand unbinding occurs after approximately 25 ns in the remaining replicate (Movies S6 and S7). For both oleacein and cyanidin-3-O-glucoside, unbinding is observed in all three replicate simulations, occurring after 10 ns for oleacein (Movie S4) and 50 ns for cyanidin-3-O-glucoside (Movie S5).

Root mean square deviation (RMSD) analysis of the protein backbone indicated that in general, systems reached equilibration after 50 ns (Figs. 6A and 7A). Subsequent analysis was performed on the stabilised trajectory following this timepoint. Average RMSD was similar between systems, with values of 0.35, 0.34, and 0.36 nm for apo, sinefungin-bound and oleuropein-bound nsp10-nsp16 complexes, respectively (Fig. 6A), indicating that binding of potential inhibitors to the SAM-binding site of SARS-CoV-2 nsp10-nsp16 does not greatly affect overall protein structure. Slightly higher average RMSD values were observed for the systems with the remaining dietary compounds where unbinding occurred (0.39 nm for oleacein, 0.38 for cyanidin-3-O-glucoside, and 0.39 for epigallocatechin gallate).

Protein backbone flexibility was examined with root mean square fluctuation (RMSF) analysis (Figs. 6C and 7C). The greatest fluctuations were observed at terminal regions of each chain of the protein complex, which can also be observed visually (Movies S1 – S7). The most prominent protein flexibility was for all systems were located at residues 20–40 and 133–143 of nsp16. These residues are located within gate loops 1 and gate loop 2 regions of the protein respectively, which function to stabilise RNA cap binding [38]. The flexibility of these residues is further highlighted in Figs. 6D and 7D, which show the difference in RMSF values of the protein backbone of ligand-bound systems following subtraction of apo values. The sinefungin-bound methyltransferase complex demonstrates a difference in RMSF of −0.10 nm at residue Asn29 and −0.09 nm at residue Val139. For oleuropein, a difference in RMSF of +0.12 nm was observed at Ser33. Epigallocatechin gallate-bound nsp16 demonstrated a difference in RMSF of +0.09 at Thr25. The cyanidin-3-O-glucoside-bound protein shows a difference in RMSF of +0.10 at Lys137 and −0.07 nm at Lys141. Another flexible region of the protein was at Arg216 and Glu217 of nsp16, which lies on the surface of the protein near the methyltransferase core [38].

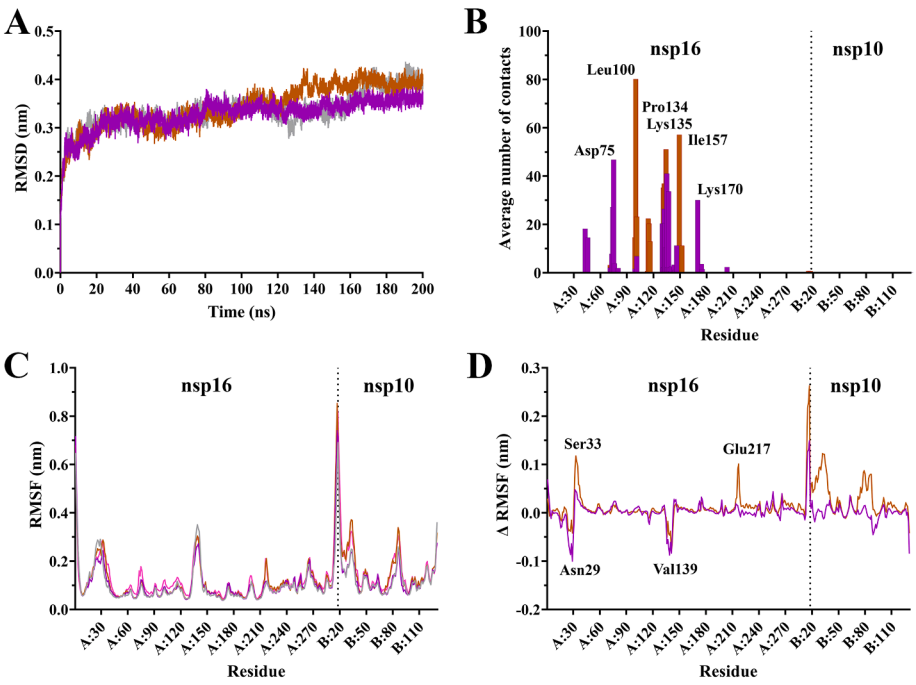

Fig. 6. Stability of SARS-CoV-2 nsp10-nsp16 methyltransferase complex bound with lead compounds. MD simulations were performed for 200 ns in triplicate for the apo form of nsp10-nsp16 (grey), and with sinefungin (purple) and oleuropein (brown) bound to the SAM-binding site. A) Average root mean square deviation (RMSD) for protein backbone with respect to its initial structure. B) Average number of contacts between the bound ligand and protein residues over a 50 ns segment of the stabilised trajectory. C) Average root mean square fluctuation (RMSF) for protein backbone over a 50 ns segment of the stabilised trajectory. D) Difference in RMSF following subtraction of apo protein backbone values from ligand-bound. (For interpretation of the references to color in this figure legend, the reader is referred to the web version of this article.)

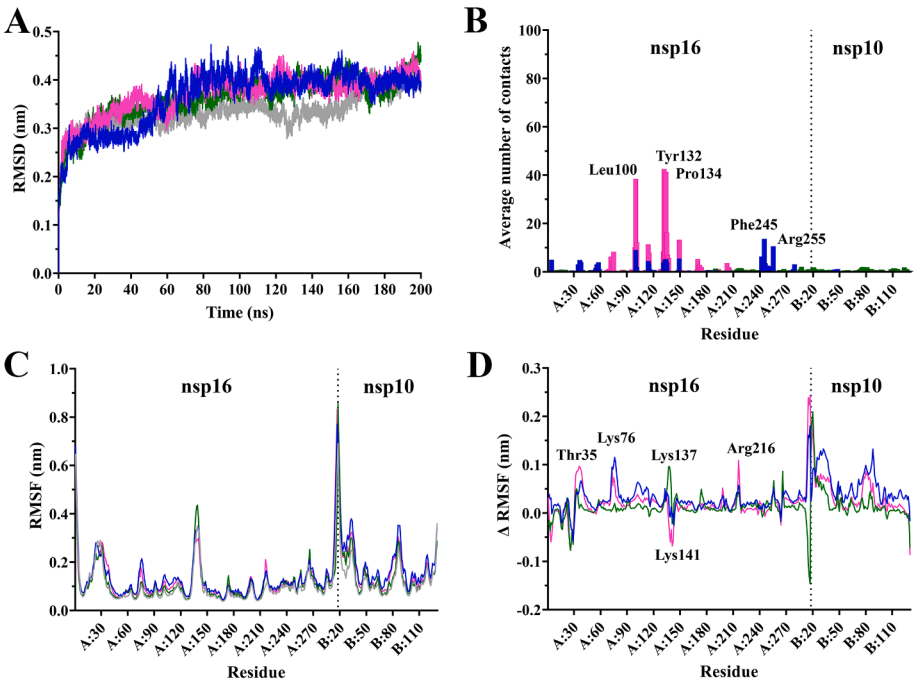

Fig. 7. Stability of SARS-CoV-2 nsp10-nsp16 methyltransferase complex bound with lead compounds. MD simulations were performed for 200 ns in triplicate for the apo form of nsp10-nsp16 (grey), and with oleacein (blue), cyanidin-3-O-glucoside (green), and epigallocatechin gallate (pink) bound to the SAM-binding site. A) Average root mean square deviation (RMSD) for protein backbone with respect to its initial structure. B) Average number of contacts between the bound ligand and protein residues over a 50 ns segment of the stabilised trajectory. C) Average root mean square fluctuation (RMSF) for protein backbone over a 50 ns segment of the stabilised trajectory. D) Difference in RMSF following subtraction of apo protein backbone values from ligand-bound. (For interpretation of the references to color in this figure legend, the reader is referred to the web version of this article.)

3.8. Residue contacts between lead compounds and protein residues

The average number of contacts over 50 ns of the stabilised trajectories between the bound ligand and protein residues was calculated in triplicate. A greater number of contacts were observed overall for sinefungin and oleuropein (Fig. 6B) compared to the remaining dietary compounds oleacein, cyanidin-3-O-glucoside, and epigallocatechin gallate (Fig. 7B). This can be attributed ligand unbinding events for the latter dietary compounds. For instance, cyanidin-3-O-glucoside was detached from the protein complex after approximately 50 ns in all three replicates and remained unbound in the solvent (Movie S5). This is demonstrated by a marked reduction in the number of contacts between the protein complex and cyanidin-3-O-glucoside (Fig. 7B). Ligand unbinding was also observed with oleacein in all three replicates, yielding a lower number of contacts with protein residues overall. Interestingly, oleacein was observed to detach from the SAM-binding site in one simulation, before re-attaching at distal sites along the protein surface (Movie S4). This is reflected by contacts with Phe245 and Arg255 in Fig. 7B, which is in line blind docking results (Fig. 5). Compared to the other dietary compounds oleacein had a lower number of poses in the SAM-binding pocket, with these residues in the proximity to the top ranked blind docking poses.

Epigallocatechin gallate which remained bound to the SAM-binding site in two replicates, demonstrates similar contacts with the most prominent residues that were making contacts with sinefungin and oleuropein. These included Leu100 (38 contacts), and gate loop 2 residues Tyr132 (42.5 contacts) and Pro134 (41.1 contacts). As mentioned above, sinefungin and oleuropein were strongly bound to the SAM-binding site of the nsp10-nsp16 protein complex for the entire trajectory. The main contacts observed with sinefungin were 46.8 contacts with Asp75 and 41.1 contacts with Lys135. Oleuropein formed the greatest number of contacts with residues Leu100 and Pro134, with an average number of 80.2 and 51.1 contacts throughout the 50 ns segment of the trajectory, respectively. These residues are involved in facilitating a favourable orientation of SAM for 2′O-methylation, suggesting that binding of oleuropein to these residues may potentially inhibit methyltransferase activity in SARS-CoV-2 nsp16 (38).

Regarding the catalytic tetrad residues of nsp16, sinefungin was the only ligand to consistently form contacts with these residues throughout the analysed trajectory. There was an average of 14.5 contacts with Lys46, 20.4 contacts with Asp130, 30.1 contacts with Lys170, and 2.4 with Glu203. All the dietary compounds were in minimal contact with these catalytic residues. While this shows that sinefungin is a strong control for inhibition of methyltransferase activity, it should be noted that it has not been developed for clinical use due to severe toxic side effects in dogs and goats [49,50]. Oleuropein, on the other hand, has been well-studied for its biological and pharmacokinetic properties as the most prominent phenolic compound found in olives [44]. Taking together molecular docking and MD simulation data from the present study, oleuropein may be a strong candidate warranting further evaluation as a potential inhibitor of methyltransferase activity in SARS-CoV-2.

4. Conclusion

Overall, a library of 300 compounds was screened for potential inhibitory properties against the nsp10-nsp16 methyltransferase complex. From a selection of 30 compounds based on binding affinity, availability, and known side effects, a more detailed docking study identified six lead compounds. These were the antiviral compounds lopinavir and ritonavir, and the dietary compounds oleuropein, oleacein, cyanidin-3-O-glucoside, and epigallocatechin gallate. MD simulations of the SARS-CoV-2 nsp10-nsp16 methyltransferase complex bound with the lead dietary compounds identified oleuropein as a potential inhibitor, requiring further evaluation using *in vitro* studies are for antiviral effects.

CRediT authorship contribution statement

Julia Liang: Formal analysis, Data curation, Writing - original draft, Writing - review & editing. **Eleni Pitsillou:** Formal analysis, Data curation, Writing - review & editing. **Lucy Burbury:** Formal analysis, Data curation, Writing - original draft, Writing - review & editing. **Andrew Hung:** Conceptualization, Methodology, Supervision, Writing - review & editing. **Tom C. Karagiannis:** Conceptualization, Methodology, Supervision, Writing - review & editing. **:** .

Declaration of Competing Interest

The authors declare that they have no known competing financial interests or personal relationships that could have appeared to influence the work reported in this paper.

Acknowledgements

We would like to acknowledge intellectual and financial support by McCord Research (Iowa, USA). JL is supported by an Australian Government Research Training Program Scholarship. We are indebted to Alfonso Perez Escudero and the team at Crowdfight COVID-19 for enabling access to supercomputing facilities, and to Matthew Gasperetti and the team at Hypernet Labs; Galileo, for enabling cloud computing for this project. We thank the National Computing Infrastructure (NCI), and the Pawsey Supercomputing Centre in Australia (funded by the Australian Government). Further, we thank the Spartan High Performance Computing service (University of Melbourne), and the Partnership for Advanced Computing in Europe (PRACE) for awarding the access to Piz Daint, hosted at the Swiss National Supercomputing Centre (CSCS), Switzerland.

Appendix A. Supplementary material

Supplementary data to this article can be found online at https://doi.org/10.1016/j.cplett.2021.138618.

References

[1] M. Nicola, Z. Alsafi, C. Sohrabi, A. Kerwan, A. Al-Jabir, C. Iosifidis, et al., The socio-economic implications of the coronavirus pandemic (COVID-19): a review, Int. J. Surg. 78 (2020) 185–193.
[2] S.P. Kaur, V. Gupta, COVID-19 vaccine: a comprehensive status report, Virus Res. 288 (2020), 198114.
[3] Coronavirus (COVID-19) Update: FDA Issues Emergency Use Authorization for Potential COVID-19 Treatment [press release], 1 May 2020.
[4] J.H. Beigel, K.M. Tomashek, L.E. Dodd, A.K. Mehta, B.S. Zingman, A.C. Kalil, et al., Remdesivir for the treatment of Covid-19 - final report, N. Engl. J. Med. 383 (19) (2020) 1813–1826.
[5] O. Dyer, Covid-19: Remdesivir has little or no impact on survival, WHO trial shows, BMJ (Clinical research ed). 371 (2020), m4057.
[6] K. Thomson, H. Nachlis, Emergency use authorizations during the COVID-19 pandemic: lessons from hydroxychloroquine for vaccine authorization and approval, JAMA 324 (13) (2020) 1282–1283.
[7] P. V'Kovski, A. Kratzel, S. Steiner, H. Stalder, V. Thiel, Coronavirus biology and replication: implications for SARS-CoV-2. Nature reviews, Microbiology (2020) 1–16.
[8] E. Petersen, M. Koopmans, U. Go, D.H. Hamer, N. Petrosillo, F. Castelli, et al., Comparing SARS-CoV-2 with SARS-CoV and influenza pandemics, Lancet Infect. Dis. 20 (9) (2020) e238–e244.
[9] A. Wu, Y. Peng, B. Huang, X. Ding, X. Wang, P. Niu, et al., Genome composition and divergence of the novel coronavirus (2019-nCoV) originating in China, Cell Host Microbe 27 (3) (2020) 325–328.
[10] A. Ramanathan, G.B. Robb, S.H. Chan, mRNA capping: biological functions and applications, Nucleic Acids Res. 44 (16) (2016) 7511–7526.
[11] E. Decroly, C. Debarnot, F. Ferron, M. Bouvet, B. Coutard, I. Imbert, et al., Crystal structure and functional analysis of the SARS-coronavirus RNA cap 2'-O-methyltransferase nsp10/nsp16 complex, PLoS Pathog. 7 (5) (2011), e1002059.
[12] Y. Chen, C. Su, M. Ke, X. Jin, L. Xu, Z. Zhang, et al., Biochemical and structural insights into the mechanisms of SARS coronavirus RNA ribose 2'-O-methylation by nsp16/nsp10 protein complex, PLoS Pathog. 7 (10) (2011), e1002294.
[13] P. Krafcikova, J. Silhan, R. Nencka, E. Boura, Structural analysis of the SARS-CoV-2 methyltransferase complex involved in RNA cap creation bound to sinefungin, Nat. Commun. 11 (1) (2020) 3717.
[14] M. Denaro, A. Smeriglio, D. Barreca, C. De Francesco, C. Occhiuto, G. Milano, et al., Antiviral activity of plants and their isolated bioactive compounds: an update, Phytother. Res.: PTR 34 (4) (2020) 742–768.
[15] C. Alarcón de la Lastra, M.D. Barranco, V. Motilva, J.M. Herrerías, Mediterranean diet and health: biological importance of olive oil, Curr. Pharm. Des. 7 (10) (2001) 933–950.
[16] E. Tazikeh-Lemeski, S. Moradi, R. Raoufi, M. Shahlaei, M.A.M. Janlou, S. Zolghadri, Targeting SARS-COV-2 non-structural protein 16: a virtual drug repurposing study, J. Biomol. Struct. Dyn. (2020) 1–14.
[17] N.P. Bonvino, J. Liang, E.D. McCord, E. Zafiris, N. Benetti, N.B. Ray, et al., OliveNet™: a comprehensive library of compounds from Olea europaea, Database (Oxford) 2018 (2018) bay016.
[18] A.A. Agbowuro, W.M. Huston, A.B. Gamble, J.D.A. Tyndall, Proteases and protease inhibitors in infectious diseases, Med. Res. Rev. 38 (4) (2018) 1295–1331.
[19] K. Gbinigie, K. Frie, Should chloroquine and hydroxychloroquine be used to treat COVID-19? A rapid review, BJGP Open 4 (2) (2020).
[20] H.P. Huemer, Possible immunosuppressive effects of drug exposure and environmental and nutritional effects on infection and vaccination, Mediators Inflamm. 2015 (2015), 349176.
[21] D.E. Kim, J.S. Min, M.S. Jang, J.Y. Lee, Y.S. Shin, J.H. Song, et al., Natural bis-benzylisoquinoline alkaloids-tetrandrine, fangchinoline, and cepharanthine, inhibit human coronavirus OC43 infection of MRC-5 human lung cells, Biomolecules 9 (11) (2019).
[22] S. Prasad, S.C. Gupta, A.K. Tyagi, B.B. Aggarwal, Curcumin, a component of golden spice: from bedside to bench and back, Biotechnol. Adv. 32 (6) (2014) 1053–1064.
[23] P. Mohammadi Pour, S. Fakhri, S. Asgary, M.H. Farzaei, J. Echeverría, The signaling pathways, and therapeutic targets of antiviral agents: focusing on the

antiviral approaches and clinical perspectives of anthocyanins in the management of viral diseases, Front. Pharmacol. 10 (2019) 1207.
[24] H. Zhou, Y. Fang, T. Xu, W.J. Ni, A.Z. Shen, X.M. Meng, Potential therapeutic targets and promising drugs for combating SARS-CoV-2, Br. J. Pharmacol. 177 (14) (2020) 3147–3161.
[25] Y. Zhou, Y. Hou, J. Shen, Y. Huang, W. Martin, F. Cheng, Network-based drug repurposing for novel coronavirus 2019-nCoV/SARS-CoV-2, Cell Discov. 6 (2020) 14.
[26] S. Kim, J. Chen, T. Cheng, A. Gindulyte, J. He, S. He, et al., PubChem 2019 update: improved access to chemical data, Nucleic Acids Res. 47 (D1) (2019) D1102–D1109.
[27] J. Liang, E. Pitsillou, C. Karagiannis, K.K. Darmawan, K. Ng, A. Hung, et al., Interaction of the prototypical α-ketoamide inhibitor with the SARS-CoV-2 main protease active site in silico: molecular dynamic simulations highlight the stability of the ligand-protein complex, Comput. Biol. Chem. 107292 (2020).
[28] J. Liang, C. Karagiannis, E. Pitsillou, K.K. Darmawan, K. Ng, A. Hung, et al., Site mapping and small molecule blind docking reveal a possible target site on the SARS-CoV-2 main protease dimer interface, Comput. Biol. Chem. 89 (2020), 107372.
[29] L. Jendele, R. Krivak, P. Skoda, M. Novotny, D. Hoksza, PrankWeb: a web server for ligand binding site prediction and visualization, Nucleic Acids Res. 47 (W1) (2019) W345–W349.
[30] O. Trott, A.J. Olson, AutoDock Vina: improving the speed and accuracy of docking with a new scoring function, efficient optimization, and multithreading, J. Comput. Chem. 31 (2) (2010) 455–461.
[31] Hypernet Labs. Galileo. Available from: <https://galileoapp.io/. 2020 [Available from: https://galileoapp.io/>.
[32] H.J.C. Berendsen, D. van der Spoel, R. van Drunen, GROMACS: a message-passing parallel molecular dynamics implementation, Comput. Phys. Commun. 91 (1) (1995) 43–56.
[33] M.J. Abraham, T. Murtola, R. Schulz, S. Páll, J.C. Smith, B. Hess, et al., GROMACS: high performance molecular simulations through multi-level parallelism from laptops to supercomputers, SoftwareX 1–2 (2015) 19–25.
[34] R.B. Best, X. Zhu, J. Shim, P.E. Lopes, J. Mittal, M. Feig, et al., Optimization of the additive CHARMM all-atom protein force field targeting improved sampling of the backbone φ, ψ and side-chain χ(1) and χ(2) dihedral angles, J. Chem. Theory Comput. 8 (9) (2012) 3257–3273.
[35] V. Zoete, M.A. Cuendet, A. Grosdidier, O. Michielin, SwissParam: a fast force field generation tool for small organic molecules, J. Comput. Chem. 32 (11) (2011) 2359–2368.
[36] M. von Grotthuss, L.S. Wyrwicz, L. Rychlewski, mRNA cap-1 methyltransferase in the SARS genome, Cell 113 (6) (2003) 701–702.
[37] M. Rosas-Lemus, G. Minasov, L. Shuvalova, N.L. Inniss, O. Kiryukhina, J. Brunzelle, et al., High-resolution structures of the SARS-CoV-2 2'-O-methyltransferase reveal strategies for structure-based inhibitor design, Sci. Signaling 13 (651) (2020).
[38] T. Viswanathan, S. Arya, S.H. Chan, S. Qi, N. Dai, A. Misra, et al., Structural basis of RNA cap modification by SARS-CoV-2, Nat. Commun. 11 (1) (2020) 3718.
[39] A.E. Cho, V. Guallar, B.J. Berne, R. Friesner, Importance of accurate charges in molecular docking: quantum mechanical/molecular mechanical (QM/MM) approach, J. Comput. Chem. 26 (9) (2005) 915–931.
[40] R.L. Hamil, M.M. Hoehn, A9145, a new adenine-containing antifungal antibiotic. I. Discovery and isolation, J. Antibiot. 26 (8) (1973) 463–465.
[41] E. Decroly, I. Imbert, B. Coutard, M. Bouvet, B. Selisko, K. Alvarez, et al., Coronavirus nonstructural protein 16 is a cap-0 binding enzyme possessing (nucleoside-2'O)-methyltransferase activity, J Virol. 82 (16) (2008) 8071–8084.
[42] B. Cao, Y. Wang, D. Wen, W. Liu, J. Wang, G. Fan, et al., A trial of lopinavir-ritonavir in adults hospitalized with severe Covid-19, N. Engl. J. Med. 382 (19) (2020) 1787–1799.
[43] Lopinavir-ritonavir in patients admitted to hospital with COVID-19 (RECOVERY): a randomised, controlled, open-label, platform trial. Lancet (London, England) 396 (10259) (2020) 1345–1352.
[44] S.H. Omar, Oleuropein in olive and its pharmacological effects, Sci. Pharm. 78 (2) (2010) 133–154.
[45] E. Cuyàs, S. Verdura, J. Lozano-Sánchez, I. Viciano, L. Llorach-Parés, A. Nonell-Canals, et al., The extra virgin olive oil phenolic oleacein is a dual substrate-inhibitor of catechol-O-methyltransferase, Food Chem. Toxicol. 128 (2019) 35–45.
[46] E. Cuyàs, J. Gumuzio, J. Lozano-Sánchez, D. Carreras, S. Verdura, L. Llorach-Parés, et al., Extra virgin olive oil contains a phenolic inhibitor of the histone demethylase LSD1/KDM1A, Nutrients 11 (7) (2019).
[47] X. Yan, L. Wu, B. Li, X. Meng, H. Dai, Y. Zheng, et al., Cyanidin-3-O-glucoside attenuates acute lung injury in sepsis rats, J. Surg. Res. 199 (2) (2015) 592–600.
[48] B.N. Singh, S. Shankar, R.K. Srivastava, Green tea catechin, epigallocatechin-3-gallate (EGCG): mechanisms, perspectives and clinical applications, Biochem. Pharmacol. 82 (12) (2011) 1807–1821.
[49] E. Zweygarth, D. Schillinger, W. Kaufmann, D. Röttcher, Evaluation of sinefungin for the treatment of Trypanosoma (Nannomonas) congolense infections in goats, Trop. Med. Parasitol. 37 (3) (1986) 255–257.
[50] M. Niitsuma, J. Hashida, M. Iwatsuki, M. Mori, A. Ishiyama, M. Namatame, et al., Sinefungin VA and dehydrosinefungin V, new antitrypanosomal antibiotics produced by Streptomyces sp. K05–0178, J. Antibiot. 63 (11) (2010) 673–679.